energies

MDPI

*Article*

# Equivalent Modeling of Microgrids Based on Optimized Broad Learning System

**Lin Wang [1,2,*] and Anke Xue [1]**

[1] School of Automation, Hangzhou Dianzi University, Hangzhou 310018, China; akxue@hdu.edu.cn
[2] School of Electrical Engineering, Yancheng Institute of Technology, Yancheng 224051, China
* Correspondence: linwang@ycit.edu.cn

**Abstract:** The DC microgrid is an important structure of microgrids. Aiming at the problem of the grid-connected DC microgrid modeling, a grid-connected DC microgrid equivalent modeling method based on the optimized Broad Learning System (BLS) is proposed. Taking the electrical parameter data of the grid-connected DC microgrid access point as the training data set of BLS, the equivalent model of the grid-connected equivalent model is constructed. In order to further improve the accuracy and generalization performance of the model, the shark smell optimization (SSO) algorithm is used to optimize the input weights and thresholds of the BLS. Furthermore, the shark smell optimization-Broad Learning System (SSO-BLS) algorithm is proposed. SSO-BLS is compared with RBF, BLS, BFO-ELM, and other algorithms. The results show that the grid-connected DC microgrid model based on SSO-BLS has good accuracy and generalization characteristics.

**Keywords:** equivalent model of grid-connected DC microgrid; optimization; broad learning system (BLS); shark smell optimization (SSO)



**Citation:** Wang, L.; Xue, A. Equivalent Modeling of Microgrids Based on Optimized Broad Learning System. *Energies* **2021**, *14*, 7911. https://doi.org/10.3390/en14237911

Academic Editors: Tek Tjing Lie and Anastasios Dounis

Received: 21 October 2021
Accepted: 22 November 2021
Published: 25 November 2021



## 1. Introduction

With the energy shortage and the improvement of environmental protection awareness, the amount of microgrids access increases year by year [1,2]. A microgrid has the advantages of high-power utilization and flexible and convenient installation which can contribute in a major way to environmental protection, improving the stability of large power grid operations and the reliability of power supply. The microgrids configurations include the AC microgrid, DC microgrid, and AC/DC hybrid microgrid. Compared with the AC microgrid, the DC microgrid reduces the power conversion link, simplifies the energy conversion process in the microgrid, and reduces the cost and power loss. DC microgrid modeling research can more comprehensively and deeply study the characteristics of microgrids, and it is also an important part of the construction of a digital twin smart grid.

The modeling methods of a microgrid are mainly divided into the component building method, equivalent electrical modeling method, and intelligent modeling method. The component building method is an early modeling method. Due to the complex internal structure of the microgrid and the difficult selection of component parameters, this method has a large workload and low fault tolerance [3,4]. The equivalent circuit method transforms the parts of microgrids into an equivalent circuit, and replaces the complex internal system of microgrids with an equivalent circuit, so as to reduce the difficulty of modeling [5–7]. The microgrids equivalent circuit modeling method is widely used in stability analysis and power flow calculation of large-scale power grid systems. The microgrid equivalent circuit modeling method is widely used in the research of large-scale power grid system stability analysis and power flow calculation. The intelligent modeling method regards the microgrid as an overall external system and uses neural networks and intelligent optimization algorithms to perform equivalent modeling of the microgrid, reducing the

complexity of modeling [8–12]. For a practical microgrid system, the equivalent model can be established only by obtaining the voltage, current, and power data of the access point.

The RBF neural network is often used, and the ELM network is often used for smart equivalent modeling of microgrids due to its simple structure, fast training speed, and strong generalization ability [13–15]. At the same time, in order to improve the model accuracy of intelligent modeling, enhance the generalization characteristics, and speed up the modeling speed, genetic algorithm [16,17], bacterial foraging algorithm [18,19], and particle swarm optimization algorithm [20,21] are often used for parameter optimization. The model established by the above microgrid intelligent equivalent modeling method can well describe the operation characteristics of the microgrid.

C. L. P. Chen proposed a BLS neural network, which has many applications because of its simple structure, few parameters, and fast calculation speed [22]. BLS has many applications, such as wind power forecasting [23] and time-series event forecasting [24]. The SSO algorithm is a new intelligent optimization algorithm. Many applications show that it has extremely high optimization efficiency [25,26]. In order to improve the accuracy of the grid-connected DC microgrid model, the SSO algorithm is used to optimize the input weight and threshold of the BLS network and the SSO-BLS neural network is constructed.

SSO-BLS is compared with RBF, BLS, BFO-ELM, and other algorithms. Refer to Section 4 for details. The results show that the grid-connected DC microgrid model based on SSO-BLS has good accuracy and generalization characteristics.

(1) We treat the DC microgrids as a whole, only collect the voltage and power of the DC microgrids grid-connected access point, and build the model, without considering the specific internal structure of the microgrid.
(2) The BLS structure is used to model the grid-connected DC microgrid, which improves the modeling accuracy and generalization characteristics.
(3) In order to further improve the accuracy of the model, the SSO-BLS algorithm is proposed. The SSO algorithm is used to optimize the $W_{ei}$ and $\beta_{ei}$ parameters of the BLS network, and thereby improving the performance of the BLS algorithm and improving the accuracy of the grid-connected DC microgrid equivalent model.

The organization of the rest of this article is as follows. Part 2 outlines the working mechanism of the BLS structure. Part 3 mainly completes the work of optimizing the BLS network based on the shark smell algorithm. Section 4 outlines the architecture of the DC microgrid model. Part 5 presents the modeling results analysis of grid-connected DC microgrid under different working conditions. Conclusions based on the study are highlighted in Section 6.

## 2. BLS

In this paper, the BLS neural network is used to realize grid-connected DC microgrid modeling, overcome the obstacles caused by the complex structure of the DC microgrid, and obtain a more accurate and fast DC microgrid modeling method. The speed of power system dynamic simulation is improved.

The BLS described in Figure 1 is a forward-type single-layer network. The input samples are mapped to feature nodes by means of linear stochastic equations so that the processing can effectively preserve the diversity of sample features. Then, all the feature nodes as a whole are mapped to an enhanced node through a nonlinear function, and then different enhanced node sets are formed. The approximation performance of the network is enhanced by this nonlinear mapping. Finally, the feature node and the enhanced node are combined as the input of the output layer. This connection method effectively reduces the loss of sample core features.

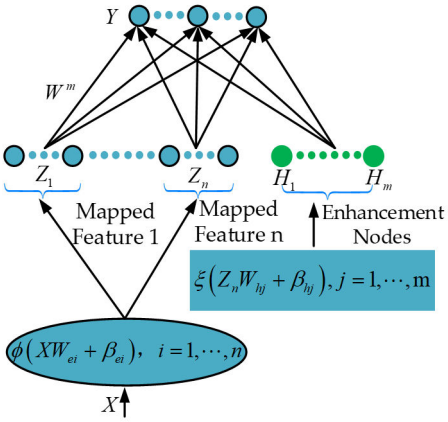


**Figure 1.** The structure of BLS.

We briefly describe the mathematical principles of BLS, which is described in more detail in [24]. Given input sample set $\{X, Y\} \in \mathbb{R}^{N\times(M+C)}$. Each feature node window $Z_i$ is obtained by the linear mapping function $\phi_i$. The mathematical formula of the $i$th feature node window is

$$Z_i = \phi_i(XW_{ei} + \beta_{ei}), i = 1, 2, \cdots, n, \tag{1}$$

where $W_{ei}$ and $\beta_{ei}$ are the weight items and bias items of the linear mapping function $\phi_i$, and they are randomly generated matrices that match the dimension of the feature node.

Denote $Z^n \triangleq [Z_1, Z_2, \cdots, Z_n]$ as feature node set. Next, $Z^n$ is used as the input of the nonlinear mapping function H to generate enhanced nodes. The $i$th enhanced node can be expressed by Equation (2)

$$H_j = \xi_j\left(XW_{hj} + \beta_{hj}\right), j = 1, 2, \cdots, m, \tag{2}$$

where $W_{hj}$ and $\beta_{hj}$ are the weight items and bias items of the nonlinear mapping function $\xi_j$. $H^m \triangleq [H_1, H_2, \cdots, H_m]$ is deemed a collection of enhanced nodes.

Hence, the network output is equivalent to Equation (3).

$$\begin{aligned} Y &= [Z_1, Z_2, \cdots, Z_n, H_1, H_2, \cdots, H_m]W^m \\ &= [Z^n, H^m]W^m \end{aligned} \tag{3}$$

where $W^m = [Z^n, H^m]^+ Y$, $W^m$ are the connection weight of the output layer and can be calculated by ridge regression.

## 3. Parameter Optimization of BLS Network

Sharks usually make path planning and capture prey through the concentration of smell particles emitted by prey. In system engineering, the target optimization is carried out by mimicking the feeding process of sharks. The SSO algorithm is combined with the BLS structure to optimize the initial parameters $W_{ei}$ and $\beta_{ei}$ of the BLS to achieve high-precision modeling of the DC microgrid, while enhancing the generalization performance of the model.

Firstly, generate the initial target value $X = [X_1, \cdots, X_T]$ in the target area, where $T$ is the number of target smell particles. We denote $X_i^1 = [x_{i,1}^1, \cdots, x_{i,j}^1]$ as the initial coordinates of the $i$-th smell particle, where j is the number of decision-making elements of smell particles, $x_{i,j}^1$ represents the coordinate of the decision element.

The SSO algorithm realizes system optimization by moving towards the direction of high particle odor concentration. The relationship between smell concentration level and target distance is expressed by fitness function L. In this algorithm, the optimization target is the initial parameters $W_{ei}$ and $\beta_{ei}$ of the BLS structure, which are expressed by the

coordinate values of smell particles. The root mean square error of the BLS training results is the basis for judging the proper performance. The root mean square error formula is

$$E = \sqrt{\frac{\sum_{i=1}^{N} \left(y_i(k) - y_i^*(k)\right)^2}{N}}, \tag{4}$$

where, $y_i(k)$ is the training output value of the BLS, $y_i^*(k)$ is the sample output value, and $N$ is the number of observations.

Generally, the greater the smell concentration of smell particles and the greater the fitness value, the better the optimization effect of SSO. We choose the reciprocal of the root mean square error as the fitness function $L$. The fitness function L uses the root mean square error. Therefore, the fitness function is as Equation (5)

$$L = 1/E, \tag{5}$$

the initial speed of shark foraging is $V^0$,

$$V^0 = \left(V_1^0, \cdots, V_i^0, \cdots V_N^0\right), \tag{6}$$

where, $V_i^0 = \left(v_{i,1}^0, \cdots, v_{i,j}^0, \cdots v_{i,M}^0\right)$, $V_i^0$ is the initial velocity of the $i$th particle, and $v_{i,j}^0$ is the $j$-dimensional initial velocity of the $i$th particle.

The movement speed of sharks while foraging increases with the increase in particle smell concentration. It is composed of the speed at the previous moment and the current acceleration, and the formula can be expressed as

$$v_{i,j}^k = \delta_k \lambda_1 v_{i,j}^{k-1} + \sigma_k \lambda_2 \frac{\partial L}{\partial x_j}\bigg|_{x_{i,j}^k}, \tag{7}$$

where, $\delta_k$, $\lambda_1$, $\lambda_2$ are random numbers uniformly distributed in the range of (0, 1), $\sigma_k$ is the $k$-th iteration inertia coefficient, $L$ is the fitness function, $k$ is the number of iterations.

The system is optimized through continuous iteration. With the increasing number of iterations, the speed of the shark will continue to increase. Therefore, it is necessary to limit the speed of the shark under the following constraints

$$\left|v_{i,j}^k\right| = \min\left[\delta_k \lambda_1 v_{i,j}^{k-1} + \left|\sigma_k \lambda_2 \frac{\partial L}{\partial x_j}\bigg|_{x_{i,j}^k}\right|, \left|\varepsilon_k v_{i,j}^{k-1}\right|\right], \tag{8}$$

where, $\delta_k$, $\lambda_1$, $\lambda_2$, $L$ have the same meaning as Equation (7), $\varepsilon_k$ is the speed limit ratio of the $k$-th iteration.

Shark foraging is realized by moving forward and rotating. The forward motion position formula is

$$Y_i^{k+1} = X_i^k + V_i^k \cdot \Delta t_k, \tag{9}$$

where, $\Delta t_k$ is the $k$th iteration time.

The position formula for the rotational motion of sharks is

$$R_i^{k+1,m} = Y_i^{k+1} + \omega \cdot Y_i^{k+1}, \tag{10}$$

where, $k$ is the number of iterations, m is the number of search points for each rotation of the shark, $\omega$ is a uniformly distributed random number in the range of $[-1, 1]$.

By searching m points near $Y_i^{k+1}$, a closed contour similar to a rotation track is formed. If the shark finds a point with a stronger smell during its rotation, it will move towards this point and continue its search. It can be expressed as

$$X_i^{k+1} = \text{argmax}\left[L\left(Y_i^{k+1}\right), L\left(Z_i^{k+1,1}\right), \cdots, L\left(Z_i^{k+1,m}\right)\right], \tag{11}$$

$X_i^{k+1}$ is the maximum fitness value of this iterative search, and it is also the starting point of the next search. The SSO algorithm is optimized by continuous iterative search to achieve the maximum number of iterations or get the ideal results.

The BLS structure has fast training speed, relatively high training accuracy, and strong generalization ability. The input weights and thresholds of the network structure are generated randomly. Considering the advantages of the SSO algorithm and BLS structure, we construct an optimized BLS algorithm, that is, the SSO-BLS algorithm.

The specific implementation steps of the SSO-BLS algorithm are as follows:

**Step1** initialization. The smell particle population is randomly generated in a specific solution space, the initial velocity vector of each particle is set, the maximum number of iterations $K_{\max}$ is set, and the optimal solution is expected to be obtained.

**Step2** Start optimization calculation. Train BLS structure to obtain the fitness value L of the population, update the speed in the process of shark optimization according to Equation (7), and conduct smell search according to Equations (9) and (10) to reach the new coordinate positions $Y_i^{k+1}$ and $R_i^{k+1,m}$ respectively.

**Step3** After completing the iterations, several optimization results will be produced by the shark's forward motion and rotating motion, and the optimal solution can be obtained from Equation (11).

**Step4** Take the output of step 3 as the input weight $W_{ei}$ and hidden layer threshold $\beta_{ei}$ of BLS, train BLS structure at the same time, and check whether the result reaches the desired optimal solution. If it is reached, the optimal solution is output; otherwise, continue to execute step 2 and cycle the optimization process until the maximum number of iterations is reached.

## 4. DC Microgrid Modeling

The SSO-BLS algorithm is applied to the Grid-connected equivalent modeling of the DC microgrid. The DC microgrid system is mainly composed of photovoltaic power, wind power, micro gas turbine, energy storage device, and load. In the DC microgrid, the AC power is connected to the DC bus through the AC/DC converter, the DC power is connected to the DC bus through the DC/DC converter, the DC load is directly connected to the DC bus or through the DC/DC converter, and the AC load is connected to the DC bus through DC/AC converter. The architecture of the DC microgrids is shown in Figure 2.

Based on the real data of the 20 kW microgrid laboratory, this paper establishes the DC grid-connected microgrid model. The main parameters of the microgrid system are shown in Table 1. The rated load is 6 kW. The experiment is carried out by adjusting the energy exchange between the microgrid and large power grid.

The architecture of the DC microgrids is complex. During operation, the grid-connected voltage and current data can better reflect the overall characteristics of the microgrid. Therefore, in the case of the AC distribution network fault, the grid-connected voltage and power data are measured to construct the data set. We take the voltage data as the input data and the power data as the corresponding output data to train the BLS structure.

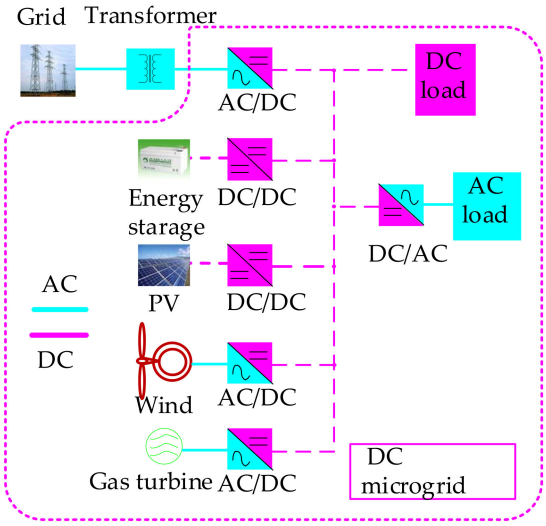


**Figure 2.** Architecture of the DC microgrids.

**Table 1.** Main parameters of the microgrids system.

| Power Generator | U | P |
|---|---|---|
| PV | 0.45 kV | 3 kW |
| wind power | 0.45 kV | 5 kW |
| micro gas turbine | 0.45 kV | 5 kW |
| energy storage | 800 Ah | |
| load | 8 kW(DC) | |

## 5. Modeling Results and Analysis

The DC microgrids are regarded as a whole, the DC microgrids are connected to the AC grid through the converters, and its equivalent model is established by taking the voltage and power of the grid-connected DC microgrid access point. At the same time, in order to verify the performance of the established model, model fitting experiments were carried out when different fault conditions such as single-phase short-circuit, two-phase short-circuit, and three-phase short-circuit occurred in the AC distribution network.

In this paper, the DC microgrids are regarded as a whole, the DC microgrids are connected to the AC distribution grid through a converter, and its equivalent model is established by taking the voltage and power of the DC microgrid grid-connected access point as the basic parameters. At the same time, in order to verify the performance of the established model, model fitting experiments were carried out when different fault conditions such as single-phase short-circuit, two-phase short-circuit, and three-phase short-circuit occurred in the AC distribution network.

The data set consists of 20,000 groups of data, including 15,000 training samples and 2000 test samples, and system failure time is set to 0.15 s.

Initialize BLS, initialize input weight matrix and threshold vector randomly, feature window N1 = 10, each window contains 10 feature nodes, and incremental node N3 = 10,000.

SSO initialization: the number of smell particles is 100, and the expected error is $e = 3.0 \times 10^{-3}$, and the maximum number of iterations is 180.

The fitting results of SSO-BLS under the condition of single-phase grounding short circuit fault in the AC distribution network are shown in Figure 3; The fitting results of SSO-BLS under the condition of two-phase short circuit fault in AC distribution network are shown in Figure 4; The fitting results of SSO-BLS under the condition of three-phase short circuit fault are shown in Figure 5. At the same time, the fitting results of BLS, BFO-ELM, RBF, and SSO-BLS are compared and analyzed.

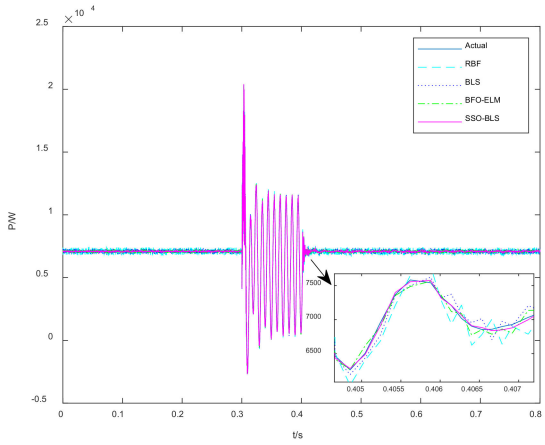


**Figure 3.** Power comparison of DC microgrids grid-connected points in AC grids with single–phase short–circuit fault.

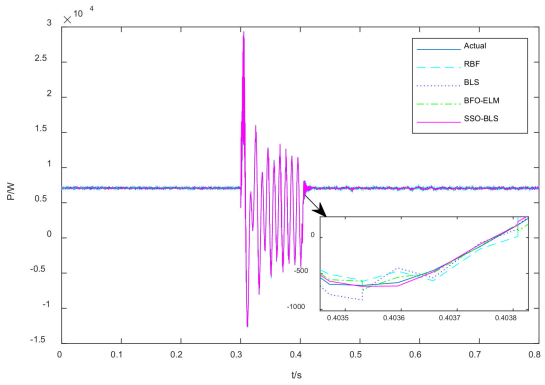


**Figure 4.** Power comparison of DC microgrids grid-connected points in AC grids with two–phase short–circuit fault.

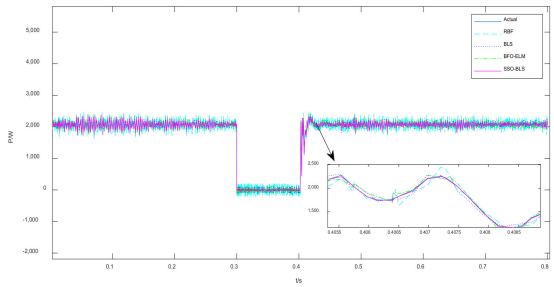

**Figure 5.** Power comparison of DC microgrids grid-connected points in AC grids with three–phase short–circuit fault.

It can be seen from Table 2 that the modeling accuracy of the RBF algorithm is relatively poor, and the BLS and BFO-ELM algorithms are close to the modeling progress, but the BFO-ELM performance is better. The modeling performance of the SSO-BLS algorithm is the best and the error is only 0.038.

**Table 2.** Average fitting error of different algorithms.

| Algorithm | Mean Root Mean Square Error |
|---|---|
| RBF | 0.3216 |
| BLS | 0.1187 |
| BFO-ELM | 0.071 |
| SSO-BLS | 0.038 |

In order to measure the difference of the DC microgrid grid-connected equivalent models established by different algorithms, the modeling errors in the interval of 0.4–0.45 s are compared, and the results are shown in Figure 6.

The internal operation conditions of DC microgrids are complex, and the load changes are diverse. In order to verify the generalization performance of the model and test the reliability of the model, the established model is applied to three different load conditions, and the results are shown in Figures 7–9. Figure 7 describes the situation that the internal loads of the microgrids are reduced by 15%. The DC microgrids can output more power to the AC grids, which shows the fitting effects of different algorithm models under this working condition. Figure 8 describes that with a 15% increase in the internal load of the microgrid, the DC microgrid consumes more electric energy and the power output to the AC microgrid decreases, which shows the fitting effect of different algorithm models under this working condition. Figure 9 shows that the internal load of DC microgrids increases by 50%, the electric energy generated in the DC microgrids can not meet the load requirements. It is necessary to absorb part of the electric energy of the AC grids to maintain the balance between power supply and load and shows the fitting effects of different algorithm models under this working condition. Figure 10 shows the comparative analysis of the model fitting results established by different algorithms when the power of the photovoltaic power plant fluctuates. As can be seen from Figures 7–10, the equivalent model based on the SSO-BLS algorithm can still well fit the operation state of microgrids under different conditions. The verification results show that the model established by the SSO-BLS algorithm has a good generalization ability and high precision, which can provide an effective guarantee for the equivalent modeling of the grid-connected DC microgrid.

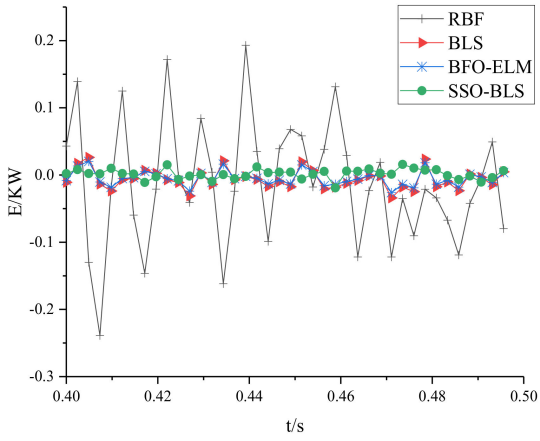


**Figure 6.** Comparison of modeling errors of different algorithms under single–phase fault condition.

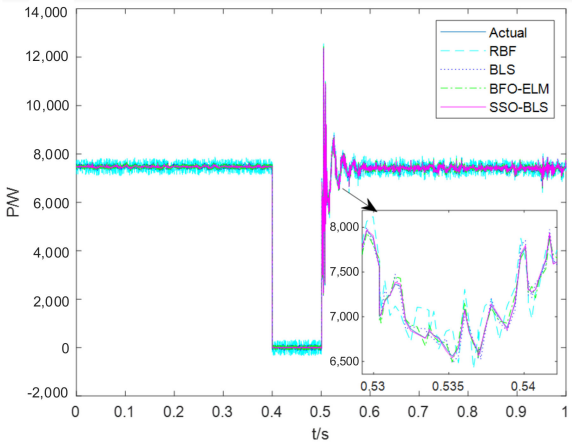


**Figure 7.** Power comparison of different equivalent models when the DC microgrids load is reduced by 15%.

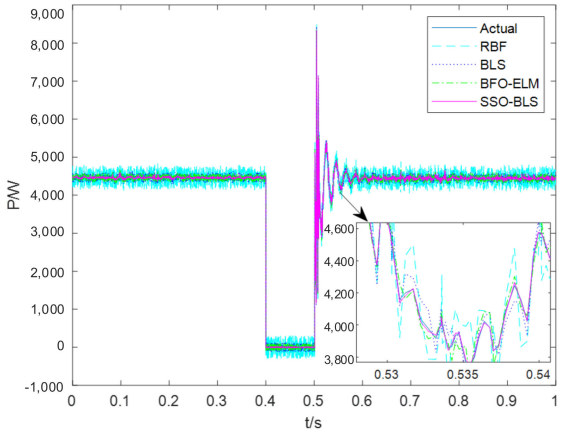


**Figure 8.** Power comparison of different equivalent models when the DC microgrids load is increased by 15%.

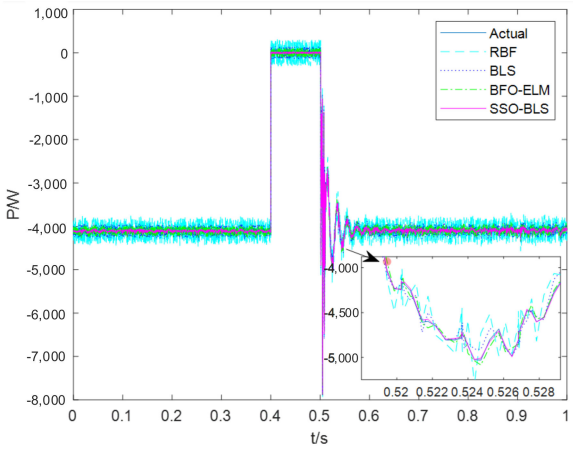


**Figure 9.** Power comparison of different equivalent models when the DC microgrids load is increased by 50%.

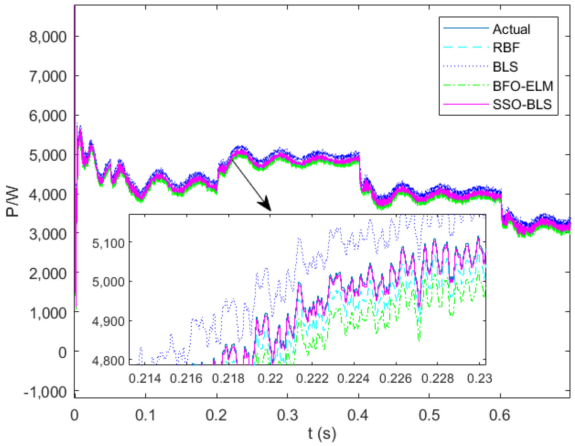


**Figure 10.** Power comparison of different equivalent models when the power of photovoltaic distributed power plants fluctuates.

## 6. Conclusions

The BLS structure is used to model the grid connection process of the DC microgrid, which is used to describe the dynamic characteristics of the grid connection operation of the DC microgrid. The shark optimization algorithm is used to optimize the input weight and threshold of the BLS structure, which not only improves the modeling accuracy

but also has good generalization performance. Under different fault conditions of the AC distribution network, the fitting results of the SSO-BLS, RBF, BLS, and BFO-ELM algorithms are compared to verify the rationality and reliability of the model.

**Author Contributions:** Conceptualization, L.W., A.X.; methodology, L.W.; software, L.W. and A.X.; validation, L.W.; formal analysis, L.W.; investigation, L.W. and A.X.; resources, L.W.; data curation, L.W.; writing—original draft preparation, L.W.; writing—review and editing, L.W. and A.X.; supervision, L.W.; project administration, L.W.; funding acquisition, L.W. All authors have read and agreed to the published version of the manuscript.

**Funding:** This research work is supported in part by Jiangsu Industry-University Project(BY2020125) by Jiangsu Chaori neng'en New Energy Technology Co., Ltd, Wuxi, China.

**Institutional Review Board Statement:** Not applicable.

**Informed Consent Statement:** Not applicable.

**Data Availability Statement:** The datasets of the current study are available from the corresponding author on reasonable request.

**Conflicts of Interest:** The authors declare no conflict of interest.

## References

1. Chen, J.; Yao, W.; Zhang, C.K.; Ren, Y.; Jiang, L. Design of robust MPPT controller for grid-connected PMSG-Based wind turbine via per-turbation observation based nonlinear adaptive control. *Renew. Energy* **2019**, *134*, 478–495. [CrossRef]
2. Jately, V.; V., B.V.; Azzopardi, S.; Azzopardi, B. Design and Performance Investigation of a Pilot Micro-Grid in the Mediterranean: MCAST Case Study. *Energies* **2021**, *14*, 6846. [CrossRef]
3. Zhou, W.; Han, L.; Li, G.; Jing, Z. Modeling and simulation of the direct-drive permanent-magnetic wind power system in microgrid based on PSCAD/EMTDC. *Electr. Technol.* **2016**, *17*, 52–57.
4. Wang, L.; Xu, D.; Zhao, H.; Hao, L.; Xu, J.; Qiu, F.; Zhang, B. Research on modeling and simulation method of direct drive permanent magnet wind power generation system. *Electron. Meas. Technol.* **2019**, *328*, 50–56.
5. Brovont, A.D.; Pekarek, S.D. Derivation and Application of Equivalent Circuits to Model Common-Mode Current in Mi-crogrids. *IEEE J. Emerg. Sel. Top. Power Electron.* **2016**, *5*, 297–308. [CrossRef]
6. Giaouris, D.; Papadopoulos, A.; Patsios, C.; Walker, S.; Ziogou, C.; Taylor, P.; Voutetakis, S.; Papadopoulou, S.; Seferlis, P. A systems approach for management of microgrids considering multiple energy carriers, stochastic loads, forecasting and demand side response. *Appl. Energy* **2018**, *226*, 546–559. [CrossRef]
7. Luna, M.; Sferlazza, A.; Accetta, A.; Di Piazza, M.C.; La Tona, G.; Pucci, M. Modeling and Performance Assessment of the Split-Pi Used as a Storage Converter in All the Possible DC Microgrid Scenarios. Theoretical Analysis. *Energies* **2021**, *14*, 5616. [CrossRef]
8. Chen, J.M.; Wang, B.; Lu, Z.X.; Shen, W.P. Photovoltaic power generation prediction based on MEA-BP neural network. In Proceedings of the 2017 32nd Youth Academic Annual Conference of Chinese Association of Automation (YAC), Hefei, China, 19–21 May 2017; pp. 387–392.
9. Cai, C.; Min, W.; Deng, L.; Zhang, J. Micro-grid dynamic modeling based on RBF Artificial Neural Network. In Proceedings of the International Conference on Power System Technology, Chengdu, China, 20–22 October 2014.
10. Lopez-Garcia, T.B.; Coronado-Mendoza, A.; Domínguez-Navarro, J.A. Artificial neural networks in microgrids: A review. *Eng. Appl. Artif. Intell.* **2020**, *95*, 103894. [CrossRef]
11. Cai, C.; Deng, L.; Bing, J.; Dai, W.; Jin, Y.; Miao, H. Micro-grid dynamic equivalent modeling based on particle swarm optimization algorithm and rbf artificial neural network. *Acta Energ Sol. Sin.* **2016**, *37*, 76–83.
12. Cai, C.; Cheng, S.; Deng, Z.; Jiang, B.; He, W.G.; Ma, J.X. DC Microgrid Equivalent Modeling Based on Fuzzy-RBF Artificial Neural Network. *Power Syst. Technol.* **2016**, *40*, 3446–3452.
13. Mishra, M.; Panigrahi, R.R.; Rout, P.K. A combined mathematical morphology and extreme learning machine techniques based approach to micro-grid protection. *Ain Shams Eng. J.* **2019**, *10*, 307–318. [CrossRef]
14. Fang, S.; Xu, Y.; Wen, S.; Zhao, T.; Wang, H.; Liu, L. Data-Driven Robust Coordination of Generation and Demand-Side in Photovoltaic Integrated All-Electric Ship Microgrids. *IEEE Trans. Power Syst.* **2019**, *35*, 1783–1795. [CrossRef]
15. Liu, N.; Zhang, Q.; Liu, H. Online short-term load forecasting based on ELM with kernel algorithm in micro-grid environment. *Diangong Jishu Xuebao/Trans. China Electrotech. Soc.* **2015**, *30*, 218–224.
16. Purnomo, D.M.; Purbarani, S.C.; Wibisono, A.; Hendrayanti, D.; Bowolaksono, A.; Mursanto, P.; Ramdhan, D.H.; Jatmiko, W. Genetic algorithm optimization for extreme learning machine based micro-algal growth forecasting of *Chlamydomonas* sp. In Proceedings of the International Conference on Advanced Computer Science & Information Systems, Depok, Indonesia, 10–11 October 2015.

17. Shanmugapriya, D.; Padmavathi, G. A wrapper based feature subset selection using ACO-ELM-ANP and GA-ELM-ANP ap-proaches for keystroke dynamics authentication. In Proceedings of the International Conference on Signal Processing Image Processing & Pattern Recognition, Coimbatore, India, 7–8 February 2013.
18. Hota, P.K.; Barisal, A.K.; Chakrabarti, R. Economic emission load dispatch through fuzzy based bacterial foraging algorithm. *Int. J. Electr. Power Energy Syst.* **2010**, *32*, 794–803. [CrossRef]
19. Dan, Y.; Tao, J. Knowledge worker scheduling optimization model based on bacterial foraging algorithm. *Futur. Gener. Comput. Syst.* **2021**, *124*, 330–337. [CrossRef]
20. Gupta, S.; Katta, A.R.; Baldaniya, Y.; Kumar, R. Hybrid Random Forest and Particle Swarm Optimization Algorithm for Solar Radia-tion Prediction. In Proceedings of the IEEE 5th International Conference on Computing Communication and Automation (ICCCA), Greater Noida, India, 30–31 October 2020.
21. Huang, Y.; Zhang, X.; Aglzim, E.-H.; Shi, L. Target 5G visible light positioning signal subcarrier extraction method using particle swarm optimization algorithm. In Proceedings of the 2021 IEEE International Symposium on Broadband Multimedia Systems and Broadcasting (BMSB), Chengdu, China, 4–6 August 2021; pp. 1–6. [CrossRef]
22. Chen, C.L.P.; Liu, Z. Broad Learning System: An Effective and Efficient Incremental Learning System without the Need for Deep Architecture. *IEEE Trans. Neural Netw. Learn. Syst.* **2018**, *29*, 10–24. [CrossRef] [PubMed]
23. Chen, C.; Liu, Z.; Feng, S. Universal Approximation Capability of Broad Learning System and Its Structural Variations. *IEEE Trans. Neural Netw. Learn. Syst.* **2019**, *30*, 1191–1204. [CrossRef] [PubMed]
24. Yang, G.; Chen, P.; Dai, L.; Yang, H. A Broad Learning System Based on Pool Computing. Available online: https://kns.cnki.net/kcms/detail/detail.aspx?doi=10.13195/j.kzyjc.2019.1729 (accessed on 20 November 2021).
25. Ahmadigorji, M.; Amjady, N. A multiyear DG-incorporated framework for expansion planning of distribution net-works using binary chaotic shark smell optimization algorithm. *Energy* **2016**, *102*, 199–215. [CrossRef]
26. Ya, W.; Russell, J.S. Parameter identification of solid oxide fuel cell by chaotic binary shark smell optimization method. *Energy* **2019**, *188*, 73–79.